Nanoscale

Large tunability in the mechanical and thermal properties of carbon nanotube-fullerene hierarchical monoliths

Journal:	*Nanoscale*
Manuscript ID	NR-COM-08-2018-006848.R3
Article Type:	Communication
Date Submitted by the Author:	16-Nov-2018
Complete List of Authors:	Giri, Ashutosh; University of Virginia, Tomko, John; University of Virginia, Mechanical and Aerospace Engineering Gaskins, John; University of Virginia, Hopkins, Patrick; University of Virginia,

ARTICLE TYPE

Cite this: DOI: 10.1039/xxxxxxxxxx

Large tunability in the mechanical and thermal properties of carbon nanotube-fullerene hierarchical monoliths†

Ashutosh Giri,*[a] John Tomko,[b‡] John T. Gaskins,[a] and Patrick E. Hopkins[ab‡a†]

Received Date
Accepted Date

DOI: 10.1039/xxxxxxxxxx

www.rsc.org/journalname

Carbon based materials have attracted much attention as building blocks in technologically relevant nanocomposites due to their unique chemical and physical properties. Here, we propose a new class of hierarchical carbon based nano-truss structures consisting of fullerene joints attached with carbon nanotubes as the truss forming a three-dimensional network. Atomistic molecular dynamics simulations allow us to systematically demonstrate the ability to simultaneously control the mechanical and thermal properties of these structures, elucidating their unique physical properties. Specifically, we perform uniaxial tensile and compressive loading to show that by controlling the length of the carbon nanotube trusses, the mechanical properties can be tuned over a large range. Furthermore, we utilize the Green-Kubo method under the equilibrium molecular dynamics simulations framework to show that the thermal conductivities of these structures can be manipulated by varying the densities of the overall structures. This work provides a computational framework guiding future research on the manipulation of the fundamental physical properties in these organic-based hierarchical structures composed of carbon nanotubes and fullerenes as building blocks.

The promise of material systems with precise control over their microstructural morphology, and those that have "user-defined" mechanical, electrical, thermal, and mass transport properties has driven an extensive thrust in the scientific community towards the design and fabrication of novel nanomaterials.[1] Carbon based materials are promising candidates as building blocks for "bottom-up" approaches in hierarchical material systems due to their different allotropes and the ability to form a wide range of geometries.[2–5] Along with the aforementioned qualities, and the added advantage of scalability, these materials can potentially offer large tunability in their physical and chemical properties with novel and systematic design of their microstructure.[6–8] Among the various allotropes are carbon nanotube (CNT) structures with rolled hexagonal carbon networks that possess enhanced mechanical, electrical, and thermal properties that have been considered for various technological applications and devices such as hydrogen storage,[9] biosensors,[10] field emission sources,[11] and flexible energy storage devices,[12] to name a few. With regards to individual CNTs, their thermal and mechanical properties stand out as they possess exceptionally high thermal conductivities of $\sim$3000 W m^{-1} K^{-1} or higher at room temperature[13–15] with ultrahigh Young's moduli of $\sim$1 TPa.[16]

As building blocks, CNTs have been joined together to form two-dimensional junctions[17,18] and three-dimensional networks[19–22] with many of the intrinsic properties of CNTs preserved in the hierarchical structures. Theoretical studies have demonstrated the ability to carefully guide electrical currents through specified paths in these hierarchical structures, which could potentially lead to CNT-based integrated electronic circuits.[23–25] Moreover, since CNTs are hard to combine with other materials and fracture upon compressive loading,[26] the introduction of chemically active fullerene molecules covalently bonded on the side walls of single-walled (SW) CNTs have shown to increase their chemical reactivity and mechanical flexibility.[27,28] In this context, it is vital that investigation towards designing and understanding the fundamental properties of new types of carbon based materials progresses with the goal of achieving novel structures capable of unearthing new regimes in materials and device design.

[a] *Department of Mechanical and Aerospace Engineering, University of Virginia, Charlottesville, Virginia 22904, USA*
[b‡] *Department of Materials Science and Engineering, University of Virginia, Charlottesville, Virginia 22904, USA*
[a†] *Department of Physics, University of Virginia, Charlottesville, Virginia 22904, USA*
† Electronic Supplementary Information (ESI) available: [Details of the computational setup, Green Kubo approach and the mechanical properties calculations]. See DOI: 10.1039/b000000x/

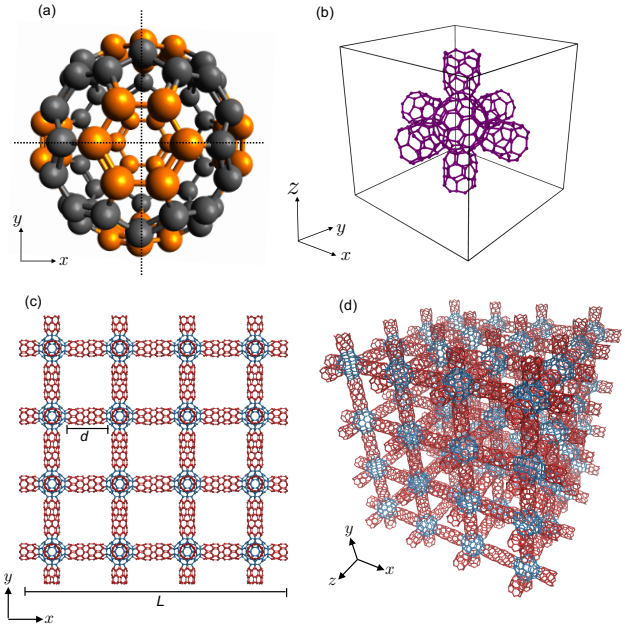

Fig. 1 (a) Schematic of the C_{80} molecule with achiral icosahedral symmetry. The orange atoms are bonded to the open ends of the (6,0) CNT. (b) A unit cell for CNT–fullerene structure with d=17.5 Å. (c) Schematic of the front view of a computational domain for a CNT–fullerene system with the CNT length of d=17.5 Å. (b) A three-dimensional view of the computational domain for the CNT–fullerene system.

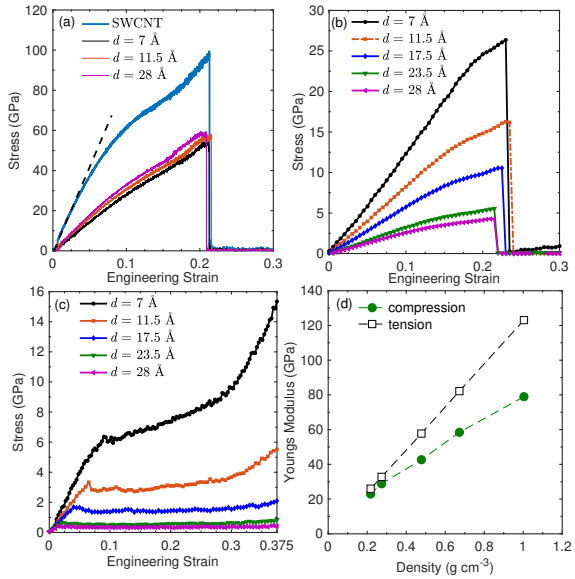

Fig. 2 (a) Stress-strain curves for a pristine (6,0) SWCNT and one-dimensional CNT-fullerene chains with varying CNT lengths under uniaxial tension. The dashed-line shows the representative linear fit to the elastic response of the pristine (6,0) SWCNT used to determine the Young's modulus. Stress-strain curves for three-dimensional CNT-fullerene structures show tunability in the Young's modulus with varying d under uniaxial (b) tension and (c) compression. (d) Young's modulus as a function of density for the CNT-fullerene systems under uniaxial tensile (hollow squares) and compressive (filled circles) loadings.

Three-dimensional CNT-based structures generally have exciting properties for applications involving biomedical devices, tough electronics, automobile industries and also offer the unique capability of significantly higher surface areas as compared to individual bundles of CNTs, which makes them idea for enhanced hydrogen storage.[22,29–32] Therefore, in this work, we present a theoretical study focusing on a new class of three-dimensional carbon based hierarchical nano-truss structures consisting of fullerene joints attached with CNTs as the trusses. We utilize atomistic simulations to demonstrate that these CNT-fullerene structures exhibit large tunability in their mechanical and thermal properties with the systematic manipulation of their microstructure. Under the molecular dynamics (MD) framework, we perform uniaxial tensile and compressive loading tests to elucidate their unique and tunable mechanical properties. We then utilize the Green-Kubo (GK) approach to predict the thermal conductivities of our structures. Our results reveal that, by controlling the length of the CNT trusses, the mechanical and thermal properties of these hierarchical monolith carbon-based nanotrusses can both be tuned by a factor of five, thus providing the knob for "user-defined" properties in these novel material systems.

Using C_{80} and (6,0) CNTs, we construct the nano-truss systems as shown in Fig. 1 by covalently bonding the fullerene and the CNT at the hexagonal rings of the fullerene and the open ends of the (6,0) CNTs. The hexagonal rings in the C_{80} that are connected to the CNT to form the nano-truss systems have been highlighted in Fig. 1a as orange atoms. The achiral icosahedral symmetry of the C_{80} molecule as shown in Fig. 1a allows the open ends of the fullerene to match with the hexagonal rings at opposite sides of the fullerene to form a three-dimensional monolith from the unit cell constructed by covalently attaching six (6,0) CNTs at the opposite ends of the C_{80} (as shown in Fig. 1b).[33] Along with the symmetry considerations, another reason for using C_{80} and (6,0) CNTs for the monoliths is also due to the fact that previous studies have demonstrated that fullerenes can be covalently attached to CNTs via the [6+6] cycloaddition, which entails bond formations of the hexagonal face of the fullerenes and six atoms in the CNT.[27,34] We vary the lengths of the CNTs (d) to create the nanotruss systems with a range of densities and porosities with d ranging from 7 to 28 Å. The size of the simulation domain ($L \times L \times L$) depends on the type of simulation (as discussed in more detail below) and is typically $104 \times 104 \times 104$ Å^3 as shown for the case of the nanotruss structure with d=17.5 Å in Figs. 1c and 1d.

Uniaxial tensile and compressive loadings are applied in the x-direction to obtain the representative stress-strain curves. Thermal conductivities are predicted utilizing the GK approach under the equilibrium molecular dynamics (EMD) simulations framework; all MD simulations are performed with the LAMMPS code[35] utilizing the widely used adaptive intermolecular reactive empirical bond-order (AIREBO) potential.[36] Additional details regarding the MD calculations used to produce deformation simulations and thermal conductivity predictions are given in the Supplementary information.

Along with our nano-truss systems, we also perform uniaxial tensile tests on individual CNTs and one-dimesional CNT-

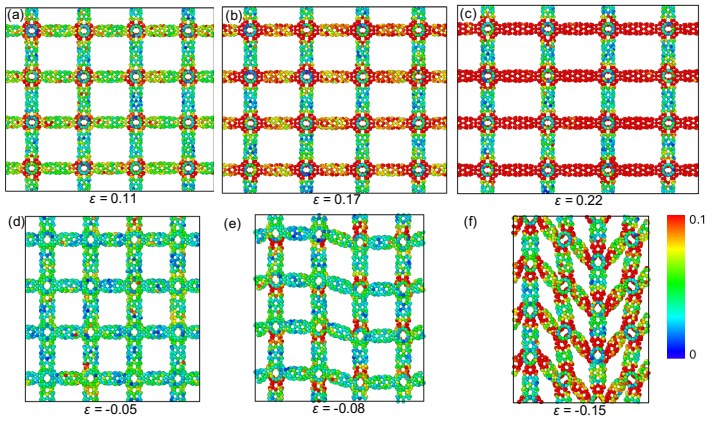

Fig. 3 Snapshots of the cross sections showing calculations of atomic level strain relative to the relaxed structure CNT-fullerene system with d=17.5 Å under uniaxial tension at (a) ε=0.11, (b) ε=0.17 and (c) ε=0.22. Similarly, snapshots at (d) ε=0.05, (e) ε=0.08 and (f) ε=0.15 for a CNT-fullerene system with d=11.5 Å under uniaxial compression.

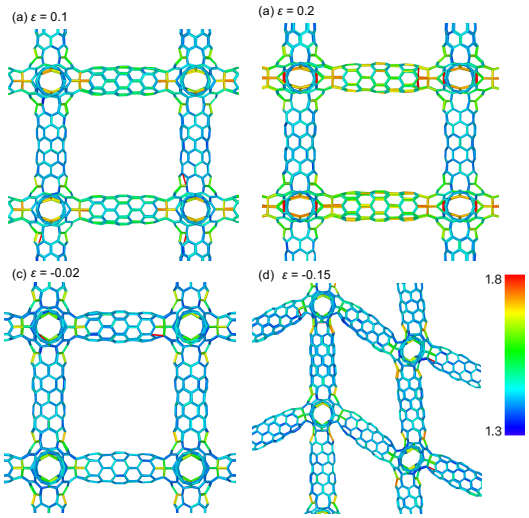

Fig. 4 Snapshots of the cross sections showing calculations of bond lengths for our CNT-fullerene structure with d=17.5 Å under uniaxial tension at (a) ε=0.1, (b) ε=0.2 and under uniaxial compression at (c) ε=-0.02 and (d) ε=-0.15. The color bar represents bond lengths from 1.3 to 1.8 Å.

fullerene chains. Figure 2a shows the stress-strain curves for the one-dimensional systems. The stress-strain curves are used to predict the Young's modulus from the slope of the linear region as shown by the dashed-line in Fig. 2a for the case of the individual CNT. In agreement with previous MD results on SWCNTs,[37–39] we predict a Young's modulus of ~0.9 TPa, which is also consistent with the experimentally determined Young's modulus for SWCNTs.[40] Also in comparison to earlier works,[37,39] a nonlinear elastic (softening) relation follows the linear behavior and fracture abruptly follows for our SWCNT. In comparison to the Young's modulus and the ultimate tensile strength of the SWCNT, the one-dimensional CNT-fullerene systems show a significant reduction in the tensile properties. It should also be noted that the Young's modulus and the ultimate tensile strength for the CNT-fullerene systems are similar to each other suggesting the length of the CNT in between the fullerene molecules does not significantly affect the tensile properties of the one-dimensional systems.

In contrast to the one-dimensional CNT-fullerene systems, the three-dimensional monoliths show a drastic change in both their Young's modulus and the ultimate tensile strengths with varying d (or porosity of the structures), as shown in the stress-strain curves in Fig. 2b. As d increases, simultaneously increasing the porosity and decreasing the density, the Young's modulus decreases, which is consistent with the mechanical behavior observed in macroporous structures of open cell foams.[41] Similarly, the Young's modulus under uniaxial compression also decreases with increasing d, as determined from the stress-strain curves in Fig. 2c. As shown in Fig. 2d, the predicted Young's modulus under both tensile and compressive forces are similar at low structure densities, while the comparative loading scenarios deviate at higher densities with the tensile specimens showing a 50% higher modulus for the highest density case. Similar linear dependence on density for our CNT-fullerene structures are also observed for the yield stresses under compressive ($\sigma_{y,T}$) and tensile ($\sigma_{y,C}$) loading, and for the ultimate tensile stress (σ_u) as tabulated in Table I.

Table 1 The length of the carbon trusses, d, densities (ρ), Young's moduli under tensile (E_T) and compressive (E_C) loading, yield stresses under tensile ($\sigma_{y,T}$) and compressive ($\sigma_{y,C}$) loading, and the ultimate tensile strengths for our CNT-fullerene structures.

d (Å)	ρ (g cm^{-3})	E_T (GPa)	E_C (GPa)	$\sigma_{y,T}$ (GPa)	$\sigma_{y,C}$ (GPa)	σ_u (GPa)
7.0	1.01	123.1	79.0	17.4	5.4	26.3
11.5	0.67	82.2	58.5	11.7	2.9	16.3
17.5	0.48	57.7	42.6	6.9	1.7	10.5
23.5	0.27	32.8	28.8	3.3	0.7	5.5
28.0	0.22	26.0	22.9	2.6	0.4	4.3

To investigate the underlying deformation mechanisms responsible for the behavior under uniaxial loading simulations, we calculate the von Mises strain associated with each atom for our structures as detailed in Ref.[42]. The local strains under uniaxial tension for the structure, with d=23.5 Å, are shown in Figs. 3a, 3b, and 3c for ε = 0.11, 0.17, and 0.22, respectively. At ε = 0.11, the structures are in the linear elastic regime and stress localization is observed for atoms adjoining the fullerenes with the carbon nanotubes as shown by the red color of the atoms, signifying a large von Mises strain. As the structure is further elongated in the x-direction, the stress concentration is distributed to neighboring atoms in the connecting CNTs along the applied strain direction and eventually the stress delocalizes throughout these CNTs and fracture of the CNTs occurs upon further applied strain. The origination and subsequent propagation of stress from the junctions between the CNTs and the fullerenes can be attributed to the transformation of the in-plane sp^2 C–C bonds into out-of-plane sp^3-like C–C bonds that are relatively more unstable.[43,44] The sp^3 bonds are also not ideal because the of the distortion in the bonding planes and the C–C bond angles. Furthermore, the interaction between triply coordinated sp^2 carbon atoms is larger than between quadruply coordinated sp^3-like carbons, making the double bonds between the carbon atoms

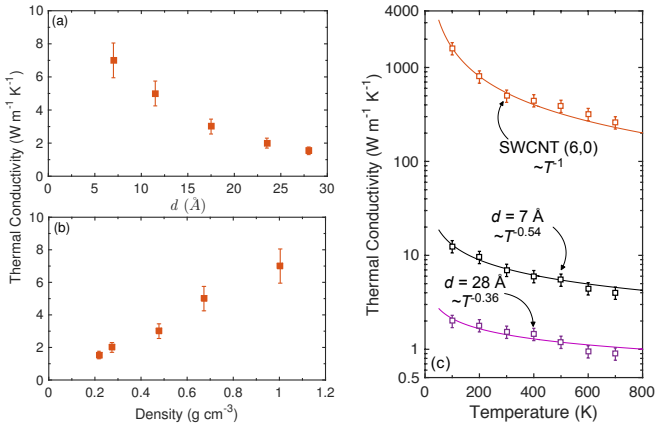

Fig. 5 MD-predicted thermal conductivities for our CNT-fullerene systems as a function of (a) length of CNT, d, and (b) density of the structures. (c) Temperature dependent thermal conductivities for CNT-fullerene systems with d= 7 and 28 Å. For comparison, the thermal conductivity for a pristine CNT that makes up the trusses is also shown.

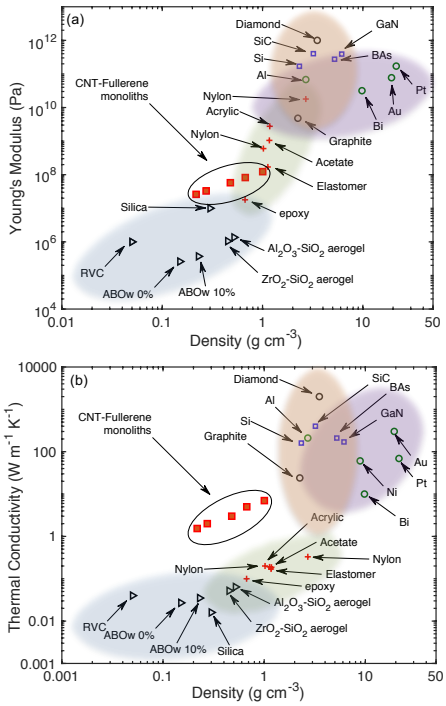

Fig. 6 (a) Comparison of (a) mechanical properties and (b) thermal properties as a function of density for our hierarchical CNT-fullerene based nano-truss structures with common aerogels, polymers, and metallic and non metallic solids.[45–51]

stronger.[36] As a result, the stretching and bending of the chemical bonds at the junctions can significantly weaken the structure making it much easier to be plastically deformed during tensile loading. Similarly, under compressive loading, stress localizations initiate at the joints as shown for the structure with d=11.5 Å in Figs. 3d and 3e by the red/yellow atoms. These stress localizations can be seen at a strain of ε=0.05, while still in a linear elastic regime and more clearly at a strain of ε=0.08, where plastic deformation of the structure, as determined from the stress-strain curve in Fig. 2c has already begun. Following the explanation above, the sp^3-like bonds that connect the CNTs with the fullerene joints are the easier bonds to bend in the structures and are therefore the ones that show the largest strain. The stress concentration at the junctions progressively leads to the bending of the stiffer CNTs, as seen in Fig. 3f), and eventually the collapse of the cells. Finally, densification of the nano-truss structures occurs whereby the stiffer CNTs come in contact with each other – in line with the abrupt increase in stress after the plastic yielding plateau region in the stress-strain relationship under compressive loading.

These results are corroborated with bond length calculations at different strain levels as shown in Fig. 4 (the bond length calculations for the entire structures are also shown in Fig. S2 of the Supporting Information). During uniaxial tensile loading, the sp^3 bonds that are formed at the connection between the fullerenes and the CNTs show drastic increase in bond lengths, indicating stress localization at these fullerene-CNT connections as shown in Fig. 4a for ε=0.1. As the stress in the structures increases due to increasing uniaxial tensile strain, the bond lengths in the entire CNT along the loading direction increases as represented in Fig. 4b for ε=0.2 (and also Fig. S2 in the Supporting Information), which results in the delocalization of the stress and ultimately leads to fracture. This energy propagation ability in the CNT results in the ductile behavior of the structure, which is similar to the stress-strain characteristic of the individual CNT as mentioned above. Note, the ductile behavior as shown in Fig. 2b is more pronounced for nanotruss structures with longer CNTs between the fullerene molecules as compared to the structure with the shortest CNT with d= 7 Å as the length of the CNTs dictates the ability to efficiently propagate the energy in the structures. Furthermore, we have carried out tensile simulations for higher strain rates as shown in Fig. S1 of the Supporting Information. Increasing the strain rate from 10^8 s^{-1} to 10^{11} s^{-1} has negligible influence on the Young's modulus, whereas, the fracture strain and fracture strength are increased due to higher strain rates, which is in line with previous simulations of tensile strain rate dependence for graphene and graphyne.[52]

In contrast to tensile loading, the sp^3 C–C bonds bend due to compressive loading as shown in Fig. 4c and Fig. 4d for ε=-0.02 and ε=-0.15, respectively, which leads to the eventual collapse of cells and densification of the structures. During the overall collapse of the cells, the sp^3 C–C bonds drastically increase in length as these bonds are the more compliant in comparison to the sp^2-like C-C bonds during the bending of the CNTs. It is interesting to note that this failure mechanism is in contrast to the stress propagation along the CNTs as observed during the failure mechanism for the tensile loading case. These different failure mechanisms during tensile and compressive loading as discussed above helps explain the differences in the Young's moduli calculated under tension and compression (as listed in Table I).

In general, large stiffness/strong bonds are often associated with high thermal conductivities. This suggests that the large

tunability in the mechanical properties of the three-dimensional CNT-fullerene structures could potentially be used as a knob to tune the thermal properties in tandem. Therefore, to understand the thermal properties, we calculate the thermal conductivities of our structures under the GK formalism that has been extensively used to predict the thermal properties of amorphous and crystalline materials alike, making it the ideal approach to predict thermal properties of our structures.[53–56] Figures 5a and 5b show the MD-predicted thermal conductivities as a function of d and density, respectively. The increase in the cell size and porosity leads to a monotonically decreasing thermal conductivity. Similar to the gradual increase in the Young's modulus with increasing density, the thermal conductivity of our structures varies by $\sim$78 % by increasing the density from 0.22 g cm^{-3} to 1.01 g cm^{-3}. These results are consistent with the density dependence of thermal conductivity observed for materials with a low volume fraction of solid, such as aerogels.[57] Moreover, the proportional relation between thermal conductivity and density is also consistent with the increasing heat conduction in solid walls of general macroscopic open cell foams with increasing density.[41]

In order to understand the intrinsic mechanism dictating thermal conductivity in these structures, we perform additional temperature dependent simulations as shown in Fig. 5c for our nano-truss structures. We compare the results to the MD-predicted thermal conductivity for a pristine CNT, which forms the walls of the structures. Consistent with the very high thermal conductivity predictions for CNTs from earlier works,[58,59] we calculate a thermal conductivity of $\sim$493$\pm$74 W m^{-1} K^{-1} for our (6,0) SWCNT. Note, the MD-predicted thermal conductivities of SWCNTs span an order of magnitude in earlier works, which has been attributed to subtle variations in computational setups and parameters utilized.[58,59] We do not try to resolve this discrepancy in the literature as our primary goal is to investigate the comparative effect of varying d on thermal properties of our hierarchical CNT-fullerene based nano-truss structures. For the pristine CNT, thermal conductivity decreases by $\sim$69% from 100 K to room temperature, whereas in comparison, the reductions in the nano-truss systems' thermal conductivities are much less pronounced. Moreover, the thermal conductivity for our pristine CNT obeys the $\sim T^{-1}$, which suggests that the scattering mechanisms are largely driven by anharmonic Umklapp scattering processes.[60] The Umklapp dominated thermal transport process for our SWCNT is consistent with the findings from prior theoretical work considering three-phonon scattering processes.[61] In contrast, the T^{-1} trend, and therefore the Umklapp dominated processes, can no longer explain the thermal conductivities of our nano-truss systems as suggested by the differing temperature dependence fits in Figs. 5c. Instead, the porosity and the cell size dictate the thermal conductivity of our nano-truss systems providing a tunable knob to control thermal transport in these novel material systems.

Finally, we compare the mechanical and thermal properties of our hierarchical CNT-fullerene based nano-truss structures with other practically relevant materials to assess the multifunctional performance of our hierarchical structures in Fig. 6. In general, both the mechanical and thermal properties of materials gradually increase with increasing density. While the densities of our structures are comparable to the densities of aerogels, the mechanical stiffness of these materials are, in most cases, orders of magnitude higher (see Fig.6a), marking a new regime of materials design that combines both ultralow densities and high stiffness, positioning them for use as functional structural materials with ultra-lightweight characteristics.[62] Similarly, in terms of thermal properties, most aerogels and polymers with similar densities to our structures have very low thermal conductivities. In contrast, our structures possess significantly higher thermal conductivities in comparison to other materials with similar densities, while simultaneously possessing a large tunable thermal conductivity range as a function of density (see Fig. 6b). The tunability in the physical properties of our hierarchical monoliths provides the opportunity for user defined combination of thermal transport and mechanical properties for various applications. For example, these structures can be used for enhanced hydrogen storage, which requires large porosities. However, our results show that care must be taken while choosing the correct morphology since large porosities can result in low thermal conductivities and reduced mechanical strengths of these structures. It is also worth noting that materials with comparable thermal conductivities and densities to our structures and those that also possess superior electrical properties as these carbon-based materials are uncommon. As such, designing material systems that exhibit such a large range of tunability in their thermal properties at these densities while maintaining (or even enhancing) the electrical performance is a formidable task, which we overcome in this work with the design of our hierarchical CNT-fullerene based nano-truss structures.

This material is based upon work supported by the Air Force Office of Scientific Research under award number FA9550-18-1-0352.

Conflicts of interest

There are no conflicts to declare.

Notes and references

1 B. D. Gates, Q. Xu, M. Stewart, D. Ryan, C. G. Willson and G. M. Whitesides, *Chemical Reviews*, 2005, **105**, 1171–1196.
2 H. Kroto, *Science*, 1988, **242**, 1139–1145.
3 S. Iijima, *Nature*, 1991, **354**, 56–58.
4 T. Kodama, M. Ohnishi, W. Park, T. Shiga, J. Park, T. Shimada, H. Shinohara, J. Shiomi and K. E. Goodson, *Nature Materials*, 2017, **16**, 892–897.
5 R. Zhou, R. Liu, L. Li, X. Wu and X. C. Zeng, *The Journal of Physical Chemistry C*, 2011, **115**, 18174–18185.
6 R. Saito, G. Dresselhaus and M. Dresselhaus, *Physical Properties of Carbon Nanotubes*, Imperial College Press, 1998.
7 R. S. Prasher, X. J. Hu, Y. Chalopin, N. Mingo, K. Lofgreen, S. Volz, F. Cleri and P. Keblinski, *Phys. Rev. Lett.*, 2009, **102**, 105901.
8 A. Giri and P. E. Hopkins, *Phys. Rev. B*, 2017, **96**, 220303.
9 C. Liu, Y. Y. Fan, M. Liu, H. T. Cong, H. M. Cheng and M. S. Dresselhaus, *Science*, 1999, **286**, 1127–1129.
10 S. Kim, J. Rusling and F. Papadimitrakopoulos, *Advanced Materials*, 2007, **19**, 3214–3228.
11 A. G. Rinzler, J. H. Hafner, P. Nikolaev, P. Nordlander, D. T. Colbert, R. E. Smalley, L. Lou, S. G. Kim and D. Tománek, *Science*, 1995, **269**, 1550–1553.
12 V. L. Pushparaj, M. M. Shaijumon, A. Kumar, S. Murugesan, L. Ci, R. Vajtai, R. J. Linhardt, O. Nalamasu and P. M. Ajayan, *Proceedings of the National Academy of Sciences*, 2007, **104**, 13574–13577.
13 P. Kim, L. Shi, A. Majumdar and P. L. McEuen, *Phys. Rev. Lett.*, 2001, **87**, 215502.
14 M. Fujii, X. Zhang, H. Xie, H. Ago, K. Takahashi, T. Ikuta, H. Abe and T. Shimizu, *Phys. Rev. Lett.*, 2005, **95**, 065502.
15 C. Yu, L. Shi, Z. Yao, D. Li and A. Majumdar, *Nano Letters*, 2005, **5**, 1842–1846.

16 M.-F. Yu, O. Lourie, M. J. Dyer, K. Moloni, T. F. Kelly and R. S. Ruoff, *Science*, 2000, **287**, 637–640.
17 M. Terrones, F. Banhart, N. Grobert, J.-C. Charlier, H. Terrones and P. M. Ajayan, *Phys. Rev. Lett.*, 2002, **89**, 075505.
18 D. Zhou and S. Seraphin, *Chemical Physics Letters*, 1995, **238**, 286 – 289.
19 W. Dacheng and L. Yunqi, *Advanced Materials*, 2008, **20**, 2815–2841.
20 J.-M. Ting and C.-C. Chang, *Applied Physics Letters*, 2002, **80**, 324–325.
21 W. Ma, L. Song, R. Yang, T. Zhang, Y. Zhao, L. Sun, Y. Ren, D. Liu, L. Liu, J. Shen, Z. Zhang, Y. Xiang, W. Zhou and S. Xie, *Nano Letters*, 2007, **7**, 2307–2311.
22 S. Ozden, G. Brunetto, N. S. Karthiselva, D. S. Galvão, A. Roy, S. R. Bakshi, C. S. Tiwary and P. M. Ajayan, *Advanced Materials Interfaces*, 2016, **3**, 1500755.
23 J. M. Romo-Herrera, M. Terrones, H. Terrones, S. Dag and V. Meunier, *Nano Letters*, 2007, **7**, 570–576.
24 J. M. Romo-Herrera, M. Terrones, H. Terrones and V. Meunier, *ACS Nano*, 2008, **2**, 2585–2591.
25 J. M. Romo-Herrera, M. Terrones, H. Terrones and V. Meunier, *Nanotechnology*, 2008, **19**, 315704.
26 B. I. Kharisov, *Recent Patents on Nanotechnology*, 2017, **11**, 235–242.
27 A. G. Nasibulin, P. V. Pikhitsa, H. Jiang, D. P. Brown, A. V. Krasheninnikov, A. S. Anisimov, P. Queipo, A. Moisala, D. Gonzalez, G. Lientschnig, A. Hassanien, S. D. Shandakov, G. Lolli, D. E. Resasco, M. Choi, D. Tománek and E. I. Kauppinen, *Nature Nanotechnology*, 2007, **2**, 156.
28 A. G. Nasibulin, A. S. Anisimov, P. V. Pikhitsa, H. Jiang, D. P. Brown, M. Choi and E. I. Kauppinen, *Chemical Physics Letters*, 2007, **446**, 109 – 114.
29 D. Wei and Y. Liu, *Advanced Materials*, 2008, **20**, 2815–2841.
30 S. Ozden, C. S. Tiwary, A. H. C. Hart, A. C. Chipara, R. Romero-Aburto, M.-T. F. Rodrigues, J. Taha-Tijerina, R. Vajtai and P. M. Ajayan, *Advanced Materials*, 2015, **27**, 1842–1850.
31 M. K. Shin, J. Oh, M. Lima, M. E. Kozlov, S. J. Kim and R. H. Baughman, *Advanced Materials*, 2010, **22**, 2663–2667.
32 G. K. Dimitrakakis, E. Tylianakis and G. E. Froudakis, *Nano Letters*, 2008, **8**, 3166–3170.
33 R. B. King and M. V. Diudea, *Journal of Mathematical Chemistry*, 2006, **39**, 597–604.
34 X. Wu and X. C. Zeng, *ACS Nano*, 2008, **2**, 1459–1465.
35 S. Plimpton, *Journal of Computational Physics*, 1995, **117**, 1–19.
36 S. J. Stuart, A. B. Tutein and J. A. Harrison, *The Journal of Chemical Physics*, 2000, **112**, 6472–6486.
37 S. Ogata and Y. Shibutani, *Phys. Rev. B*, 2003, **68**, 165409.
38 K. M. Liew, C. H. Wong, X. Q. He, M. J. Tan and S. A. Meguid, *Phys. Rev. B*, 2004, **69**, 115429.
39 R. Rafiee and M. Mahdavi, *Proceedings of the Institution of Mechanical Engineers, Part L: Journal of Materials: Design and Applications*, 2016, **230**, 654–662.
40 A. Krishnan, E. Dujardin, T. W. Ebbesen, P. N. Yianilos and M. M. J. Treacy, *Phys. Rev. B*, 1998, **58**, 14013–14019.
41 L. J. Gibson and M. F. Ashby, *Cellular Solids: Structure and Properties*, Cambridge University Press, 2nd edn, 1997.
42 F. Shimizu, S. Ogata and J. Li, *Materials Transactions*, 2007, **48**, 2923–2927.
43 L. Xu, N. Wei, Y. Zheng, Z. Fan, H.-Q. Wang and J.-C. Zheng, *J. Mater. Chem.*, 2012, **22**, 1435–1444.
44 W. M. Ji, L. W. Zhang and K. M. Liew, *EPL (Europhysics Letters)*, 2018, **121**, 56001.
45 G. Slack, *Journal of Physics and Chemistry of Solids*, 1973, **34**, 321 – 335.
46 J. E. Field, *Crystal Research and Technology*, 1992, **28**, 602–602.
47 . Harris, Gary Lynn, I. of Electrical Engineers and I. I. service), *Properties of silicon carbide*, London : INSPEC, 1995.
48 A. Polian, M. Grimsditch and I. Grzegory, *Journal of Applied Physics*, 1996, **79**, 3343–3344.
49 M. A. Hopcroft, W. D. Nix and T. W. Kenny, *Journal of Microelectromechanical Systems*, 2010, **19**, 229–238.
50 D. R. Lide, *CRC Handbook for Chemistry and Physics*, CRC Press/Taylor and Francis, Boca Raton, FL, Internet Version edn, 2008.
51 R. B. Ross, *Metallic Materials Specification Handbook*, Springer, 4th edn, 1992.
52 Y.-Y. Zhang, Q.-X. Pei, Y.-W. Mai and Y.-T. Gu, *Journal of Physics D: Applied Physics*, 2014, **47**, 425301.
53 M. P. Allen and D. J. Tildesley, *Computer simulation of liquids (Oxford Science Publications)*, Oxford University Press, Reprint edn, 1989.
54 A. McGaughey and M. Kaviany, *International Journal of Heat and Mass Transfer*, 2004, **47**, 1783 – 1798.
55 A. McGaughey and M. Kaviany, *International Journal of Heat and Mass Transfer*, 2004, **47**, 1799 – 1816.
56 A. J. H. McGaughey, *PhD thesis*, University of Michigan, 2004.
57 P. E. Hopkins, B. Kaehr, E. S. Piekos, D. Dunphy and C. Jeffrey Brinker, *Journal of Applied Physics*, 2012, **111**, 113532.
58 R. N. Salaway and L. V. Zhigilei, *International Journal of Heat and Mass Transfer*, 2014, **70**, 954 – 964.
59 J. R. Lukes and H. Zhong, *Journal of Heat Transfer*, 2006, **129**, 705–716.
60 J. M. Ziman, *Electrons and Phonons*, Clarendon Press, Oxford, 1960.
61 J. X. Cao, X. H. Yan, Y. Xiao and J. W. Ding, *Phys. Rev. B*, 2004, **69**, 073407.
62 L. R. Meza, S. Das and J. R. Greer, *Science*, 2014, **345**, 1322–1326.

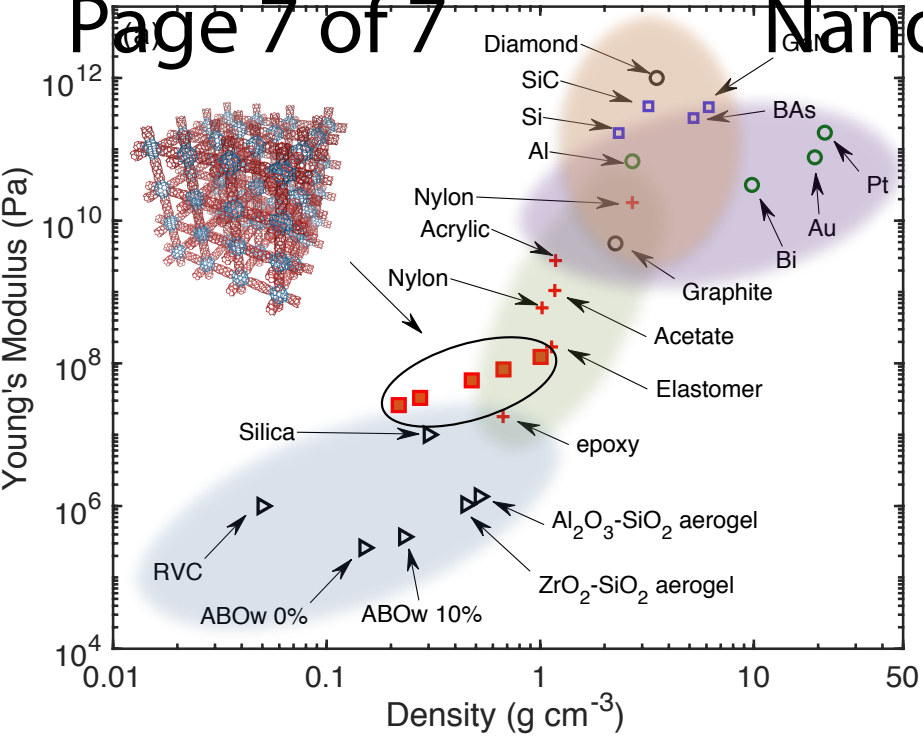
(a)
Diamond
SiC
Si
Al
GaN
BAs
Pt
Au
Bi
Nylon
Acrylic
Graphite
Acetate
Elastomer
epoxy
Silica
Al_2O_3-SiO_2 aerogel
ZrO_2-SiO_2 aerogel
RVC
ABOw 0%
ABOw 10%
Young's Modulus (Pa)
Density (g cm^{-3})

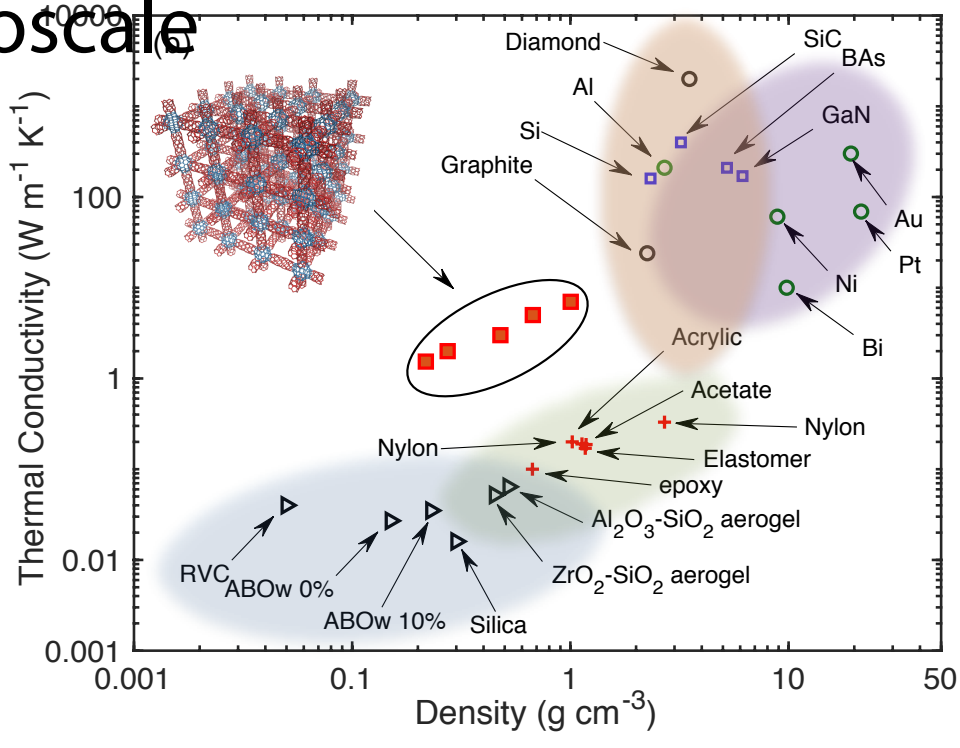
(b)
Diamond
SiC
BAs
Al
GaN
Si
Graphite
Au
Pt
Ni
Bi
Acrylic
Acetate
Nylon
Elastomer
epoxy
Al_2O_3-SiO_2 aerogel
ZrO_2-SiO_2 aerogel
RVC
ABOw 0%
ABOw 10%
Silica
Thermal Conductivity (W m^{-1} K^{-1})
Density (g cm^{-3})